ACS Photonics

Article

pubs.acs.org/journal/apchd5

# Quantum Dots in Two-Dimensional Perovskite Matrices for Efficient Near-Infrared Light Emission

Zhenyu Yang,[†] Oleksandr Voznyy,[†] Grant Walters,[†] James Z. Fan,[†] Min Liu,[†] Sachin Kinge,[‡] Sjoerd Hoogland,[†] and Edward H. Sargent*[,†]

[†]The Edward S. Rogers Department of Electrical and Computer Engineering, University of Toronto, 10 King's College Road, Toronto, Ontario M5S 3G4, Canada

[‡]Advanced Technology Materials and Research, Research and Development, Toyota Technical Centre, Hoge Wei 33, B-1930, Zaventem, Belgium

Supporting Information

**ABSTRACT:** Quantum-dot-in-perovskite solids are excellent candidates for infrared light-emitting applications. The first generation of dot-in-perovskite light-emitting diodes (LEDs) has shown bright infrared electroluminescence with tunable emission wavelength; however, their performance has been limited by degradation of the active layer at practical operating voltages. This arises from the instability of the three-dimensional (3D) organolead halide perovskite matrix. Herein we report the first dot-in-perovskite solids that employ two-dimensional (2D) perovskites as the matrix. 2D perovskite passivation is achieved via an in situ alkylammonium/alkylamine substitution carried out during the quantum dot (QD) ligand exchange process. This single-step film preparation process enables deposition of the QD/perovskite active layers with thicknesses of 40 nm, over seven times thinner than the first-generation dot-in-perovskite thin films that relied on a multistep synthesis. The dot-in-perovskite film roughness improved from 31 nm for the first-generation films to 3 nm for films as a result of this new approach. The best devices exhibit external quantum efficiency peaks exceeding 2% and radiances of ~1 W $sr^{-1}$ $m^{-2}$, with an improved breakdown voltage up to 7.5 V. Compared to first-generation dot-in-perovskites, this new process reduces materials consumptions 10-fold and represents a promising step toward manufacturable devices.

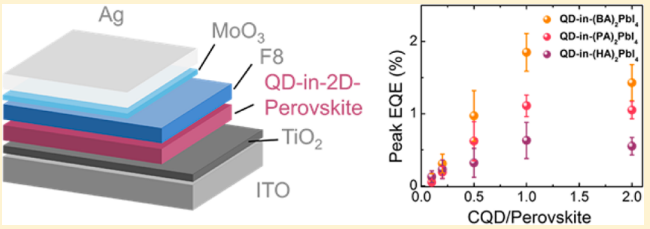


**KEYWORDS:** *quantum dots, perovskites, light-emitting diodes, infrared light emission*

Colloidal quantum dots (QDs)[1,2] exhibit size-tunable luminescence, narrow emission line width, high photoluminescence quantum yield, and excellent photostability. As a result, they are promising candidates for light-emission applications.[3−9] Solution-processed QD-based light-emitting diodes (LEDs) have shown high efficiency and high brightness with electroluminescence in both the visible and near-infrared (NIR) spectral regimes. These features compare well with those of polymer and organics LEDs.[6,10−15] Continued advances in both charge-transporting and light-emitting materials have resulted in improved carrier confinement and radiative recombination in the QD layers leading to continued efficiency improvements.

Solution-processed QD-based LEDs employ a double-heterojunction architecture in which the emissive QD layer is sandwiched between an electron transport layer (ETL) and a hole transport layer (HTL). A high efficiency of radiative recombination within QD cores is achieved via an efficiency of charge injection and blocking provided by both the ETL and HTL and also depends on the QD photoluminescence quantum efficiency (PLQE).[16] Although NIR QD solutions have luminescence efficiencies that reach ~40%,[17] the PLQEs of corresponding QD films are much lower due to nonradiative recombination and the dissociation of charge carriers at surface defects and material interfaces.[18,19] Several strategies exist to avoid the PL self-quenching effect, such as the preparation of type-I core−shell heterostructures or encapsulation using inorganic semiconductors or polymer matrices.[6,20−22] These strategies, however, introduce barriers to charge transport that increase device operating voltages and therefore power consumption.

Recently introduced quantum-dot-in-perovskite heterocrystals are a promising platform for NIR QD-LEDs.[23] The type-I dot-in-perovskite heterostructure enables efficient radiative recombination within the embedded QDs via charge injection from the high-mobility three-dimensional (3D) organolead halide perovskite matrix. With the increased charge carrier diffusion length provided by the perovskite matrix, and the epitaxial match to the QDs, dot-in-perovskite thin films have shown efficient charge transport without compromise to PLQE. The corresponding devices showed high radiance and a power conversion efficiency of 5.2%, a new record among NIR QD-

**Received:** November 3, 2016
**Published:** March 13, 2017





DOI: 10.1021/acsphotonics.6b00865
*ACS Photonics* XXXX, XXX, XXX−XXX

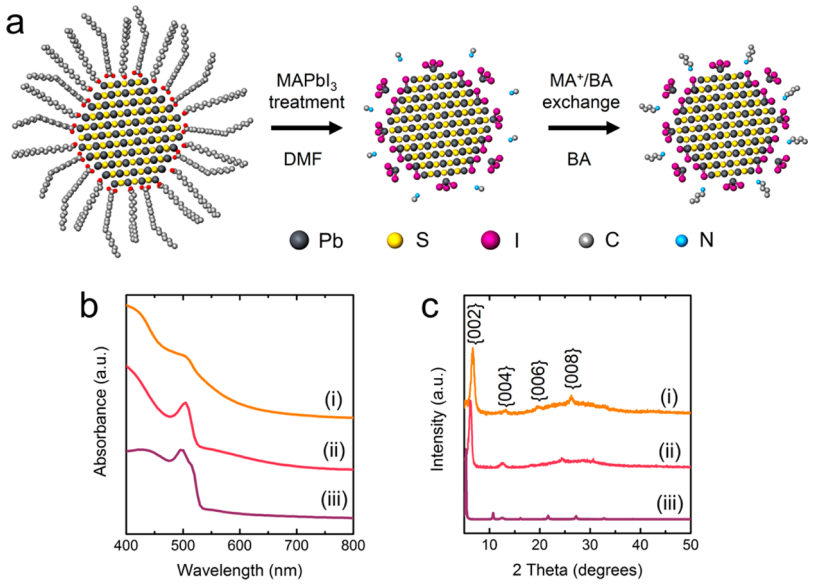


**Figure 1.** (a) Schematic showing the PbS surface ligand exchange from original OA to 3D perovskite and 2D perovskite passivation in solution. (b) Absorption spectra and (c) XRD patterns of dot-in-perovskite films fabricated with different types of amine solvents: (i) BA, (ii) PA, and (iii) HA. Crystal signals assigned to 2D perovskite are labeled in black (PbS/perovskite mass ratio: 1:1).

LEDs.[16] Unfortunately, these 3D organolead based perovskite matrices, such as methylammonium lead halide ($MAPbX_3$, X = Cl, Br, I), suffer from low stability to heat and moisture. This arises from their low formation energy and the vibration of the methylammonium cations.[24] The low stability leads to the gradual decomposition of the perovskite crystals under forward bias and causes the dot-in-perovskite hybrid LEDs to break down at a relatively low voltage of ~4.5 V.[16]

The formation energy of perovskites is, in part, determined by the choice of the monovalent organoamine group.[25] Substitution of the methylammonium cation ($CH_3NH_2^+$) with other alkylammonium groups ($R\text{-}NH_2^+$) with longer carbon backbones breaks the symmetry of the 3D structure and introduces two-dimensional (2D) structuring layered along the *c*-axis. The layering increases the crystal formation energy and produces a perovskite structure more resilient to moisture and irradiation.[26] We therefore investigated a new ligand exchange approach to encapsulate PbS QDs using 2D perovskites. We explored a range of alkylammonium ligands to form a next-generation dot-in-perovskite solid (i.e., quantum-dot-in-2D-perovskite) for LED applications. We introduced three types of 2D perovskites using a new amine/ammonium solution exchange process.[27] The dot-in-2D-perovskite thin films were prepared by spin-casting a solution containing QDs and perovskite precursors, and then annealing the films. The surface roughness of the films is far lower than that of first-generation (i.e., QD-in-3D-perovskites) films. The best LEDs exhibit external quantum efficiency (EQE) peak values up to 2% and radiances of ~1 W $sr^{-1}$ $m^{-2}$. Devices maintain high performance (radiance >0.7 W $sr^{-1}$ $m^{-2}$) at operation voltages up to 7.5 V, a 1.7× improvement over the previous dot-in-perovskite LEDs (the latter exhibited a breakdown bias of ~4.5 V). The active layer film roughness is improved from 31 nm for the first-generation films to 3.0 nm for films based on the new-generation approach. This new process reduces materials consumptions 10-fold and represents a promising step toward manufacturable dot-in-perovskite devices.

## RESULTS AND DISCUSSION

The ligand exchange process to encapsulate PbS QDs using 2D perovskite precursors is shown in Figure 1a. QDs emitting in the infrared were synthesized following a modified hot injection method (experimental section).[28] The oleic acid (OA) surface ligands were exchanged with perovskite ligand precursors (MAI + $PbI_2$) and were further removed by subsequent purification processing. The $MAPbI_3$-capped QDs are highly soluble in hydrophilic volatile alkylamine solvents such as butylamine (BA), pentylamine (PA), and hexylamine (HA). The desired amount of perovskite precursors (i.e., $PbI_2$ and MAI) was added to the alkylamine solvent. This solution was then mixed with the exchanged QD solution. During the redispersion, amine molecules substituted the $MA^+$ cations serving as ligands such that alkylammonium lead iodide formed on the PbS QDs. The QDs exchanged with the perovskite precursors were finally spin-cast onto glass substrates and annealed at 70 °C under an inert atmosphere.

The 3D-to-2D perovskite transformation was confirmed using absorption spectroscopy (Figure 1b). $MAPbI_3$ has a characteristic broad absorption across the entire visible spectrum, a behavior not observed in the spectra of the exchanged QD films. For the exchanged films, we only observed absorption features of 2D perovskites, ranging from 498 to 510 nm, depending on the applied alkylamine species. The slight blueshift of the absorption feature of 2D perovskites from $(BA)_2PbI_4$ (510 nm) to $(HA)_2PbI_4$ (498 nm) is consistent with the increasing *d*-spacing between adjacent $PbI_4^{2-}$ octahedral layers associated with the size of the alkylammonium cations.

The crystallinity change from pure QDs to dot-in-perovskite solids was verified using X-ray diffraction (XRD). The XRD pattern of the film of QDs after MAI and $PbI_2$ ligand exchange is dominated by PbS signals (Figure S1). After the alkylamine treatment and dot-in-pervoskite film process, layered structure perovskite signals are evident at two-theta angles below 10° (Figure 1c). The high intensity and the narrow spread of the signals assigned to the perovskite (00*l*) planes suggest the


DOI: 10.1021/acsphotonics.6b00865
ACS Photonics XXXX, XXX, XXX−XXX

formation of large crystal domains. We also notice the shift of the {002} signals to lower angles as the length of the alkylammonium chains are increased: {002} signals at 6.7°, 6.2°, and 5.4° for $(BA)_2PbI_4$, $(PA)_2PbI_4$, and $(HA)_2PbI_4$ matrices, respectively. This trend is consistent with the expansion of the unit cell of the 2D perovskite along the *c*-axis (*c*-axis lattice constant: $(BA)_2PbI_4$: 27.601 Å, $(PA)_2PbI_4$: 14.881 Å (monoclinic) and 29.956 Å (orthorhombic), $(HA)_2PbI_4$: 32.703 Å).[29] PbS QD features at ∼25° and ∼32°, which correspond to {111} and {200} lattice planes, are relatively weak due to dilution by the perovskite and only can be found when high concentration of QDs are present in the dot-in-perovskite film (Figure S2). The volatility of the amine source is key to the formation of the 2D perovskite matrix: alkylamines with carbon numbers below four (e.g., propylamine) are too volatile to yield a crystallized and uniform QD-perovskite film from the postspin-casting process.

Transmission electron microscope (TEM) imaging gives details about the QD surface before and after passivation. Figure 2a confirms that the postsynthesized OA-capped QDs

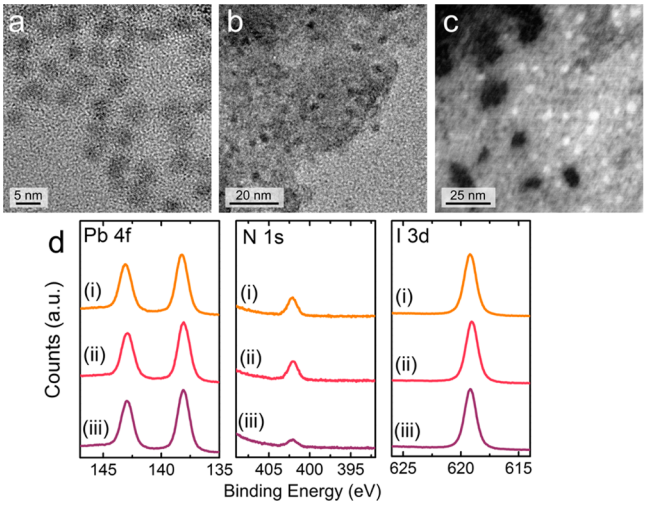


**Figure 2.** High resolution TEM images of (a) OA-capped PbS and (b) PbS in $(BA)_2PbI_4$ 2D perovskite matrix. (c) STEM-HAADF image of PbS QDs embedded in $(BA)_2PbI_4$ matrix. (d) High-resolution XPS results of lead 4f, nitrogen 1s, and iodine 3d for different types of dot-in-perovskite films: (i) BA, (ii) PA, and (iii) HA (PbS/perovskite mass ratio: 1:1).

are uniform in size (∼3.1 nm). After the ligand exchange and encapsulation with perovskite ligands and crystals, PbS QDs are well dispersed in the matrix (Figure 2b). The PbS (high-contrast spots) and perovskite domains (the matrix) are distinguishable under scanning transmission electron microscope high-angle annular dark-field (STEM-HAADF) imaging (Figure 2c). X-ray photoelectron spectra (XPS) of the annealed dot-in-perovskite films show the presence of lead 4f (143.1 and 138.2 eV for $4f_{5/2}$ and $4f_{7/2}$, respectively), nitrogen 1s (402.3 eV) and iodine 3d (619.0 eV), and show their oxidation states are well-aligned with the literature results.[30,31] Moreover, compositional ratios among Pb, N, and I from those films with different matrices are consistent with the stoichiometry of the corresponding 2D perovskites (Table S1). The 2D perovskite matrix passivates the QD surfaces without causing QD agglomeration and material phase segregation. This is reflected by the increase in PL lifetime from subnanosecond (on pure PbS thin film[23]) to over 700 ns measured on dot-in-perovskite matrix film in this study (Figure S3).

We fabricated devices with the architecture shown in the cross-sectional image of Figure 3a. The QD-perovskite mixed solution was spin-cast onto $TiO_2$ prepatterned indium tin oxide (ITO) substrates and annealed at 70 °C under an inert atmosphere to yield the emissive layer. The HTL material poly(9,9-dioctylfluorene) (F8) and the top electrode pair ($MoO_3$ + Ag) were added by spin-casting and thermal evaporating, respectively. The devices' energy band diagram is shown in Figure 3b. The valence bands (VB) and conduction bands (CB) of PbS QDs lie within the bandgap of 2D perovskites ($E_g$ = 2.4 eV) and so form the typical type-I semiconductor heterostructure. The energy levels of F8 and $TiO_2$ are well-aligned with the QD-perovskite band edges and so provide great electron and hole blocking functions, respectively. Cross-sectional scanning electron microscope (SEM) imaging revealed the total thickness of the device is around 200 nm ($TiO_2$: ∼20 nm, QD-perovskite thin film: ∼40 nm, F8:30 nm, $MoO_3$ + Ag: ∼100 nm). This single-step film preparation process enables the fabrication of dot-in-perovskite active layers with thicknesses of 40 nm, over seven times thinner than the active layer in the first-generation dot-in-perovskite devices (300 nm) and with much better film smoothness. Atomic force microscopy (AFM) confirmed the surface roughness (Rq) of the active layer (on top of the $TiO_2$/ITO substrate) was around 3.0−6.6 nm depending on the amine source (Figures 2d and S4 and Table S2), much smaller than that of the first generation of dot-in-perovskite films prepared as reported with the two-step method (RMS roughness = 30.9 nm, Figure S5).[16]

The absorption exciton peak of the starting OA-capped PbS QD solution was at approximately 1060 nm. After perovskite exchange, encapsulation and film preparation, the final electroluminescence (EL) maximum of the device was around 1280 nm (Figure 3d). Device performance depends strongly on the QD/perovskite ratio. The optimal EQE is attained with a 50% weight percent of QDs within the emissive layer (i.e., QD/perovskite weight ratio = 1:1), regardless of the type of ammonium used to construct the 2D perovskite (Figure 3a). We also notice that the EQE results of the devices with $(BA)_2PbI_4$ perovskite matrix surpasses the other two types of dot-in-perovskite LEDs (Figure 4a,b). This may originate from the decrease of the overall matrix conductivity as the organic monovalent cations become bulkier inside the perovskite matrices, causing inefficient charge injection and transport inside the active layer.

XRD patterns of dot-in-perovskite films stored in air for 2 weeks do not show any new signals due to $PbI_2$, a common byproduct from the decomposition of 3D $MAPbI_3$ perovskite (Figures S6 and S7). This suggests that 2D perovskite matrices are more stable when exposed to moisture and air. The enhanced stability is also seen in the fact that the devices were capable of operation at biases up to 7.5 V, a 1.7× improvement over the previous dot-in-perovskite LEDs, where the latter have breakdown voltage of ∼4.5 V.[16] Moreover, since the QD ratio within these films is significantly higher than that for the first generation of dot-in-perovskite devices (i.e., 50% vs, 3.6%). The radiance of 0.95 W $sr^{-1}$ $m^{-2}$ is comparable to that of the first generation device, even though the active layer is over 7× thinner.[16] This also suggests that the dispersity of QDs inside the 2D perovskite matrix at high QD mass ratios, regardless of


DOI: 10.1021/acsphotonics.6b00865
ACS Photonics XXXX, XXX, XXX−XXX

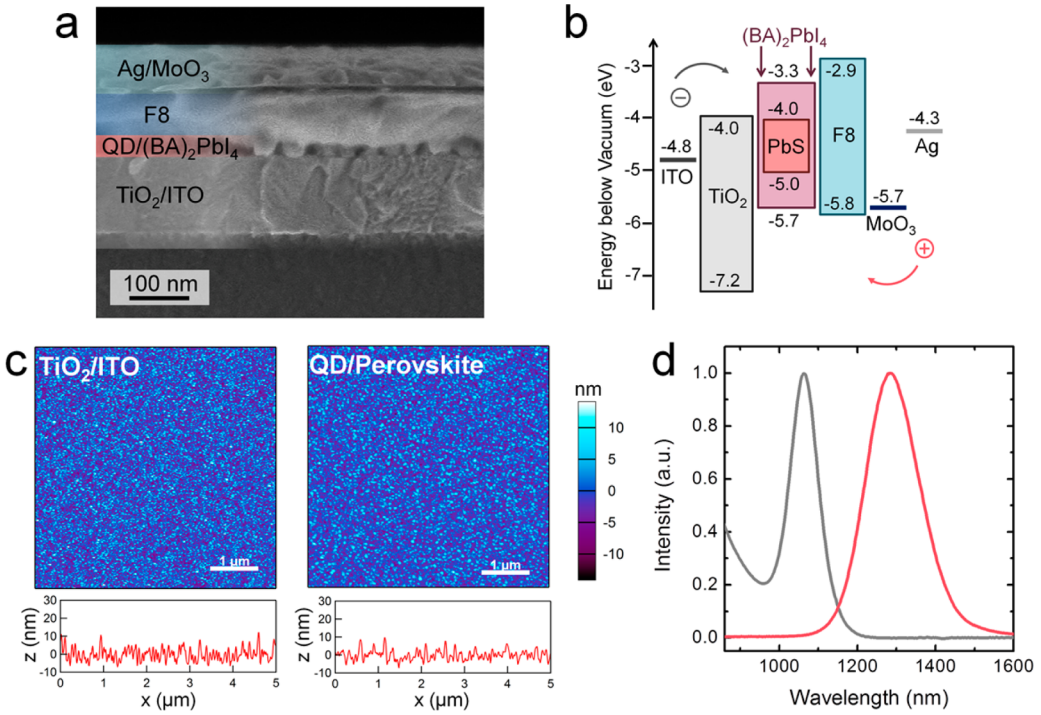


**Figure 3.** (a) Cross-sectional SEM image and (b) band diagram of the quantum-dot-in-2D-perovskite device. The band alignment of $(BA)_2PbI_4$ was estimated based on published literature.[34,35] (c) AFM images of the (left) ETL ($TiO_2$ on ITO substrate) and (right) dot-in-$(BA)_2PbI_4$ active layer spin-cast on top of the ETL. The corresponding cross-sectional height profiles are shown below the images. (d) Absorption spectra of original OA-capped PbS CQDs (gray) and electroluminescence spectra of the corresponding 2D-perovskite passivated PbS film (red).

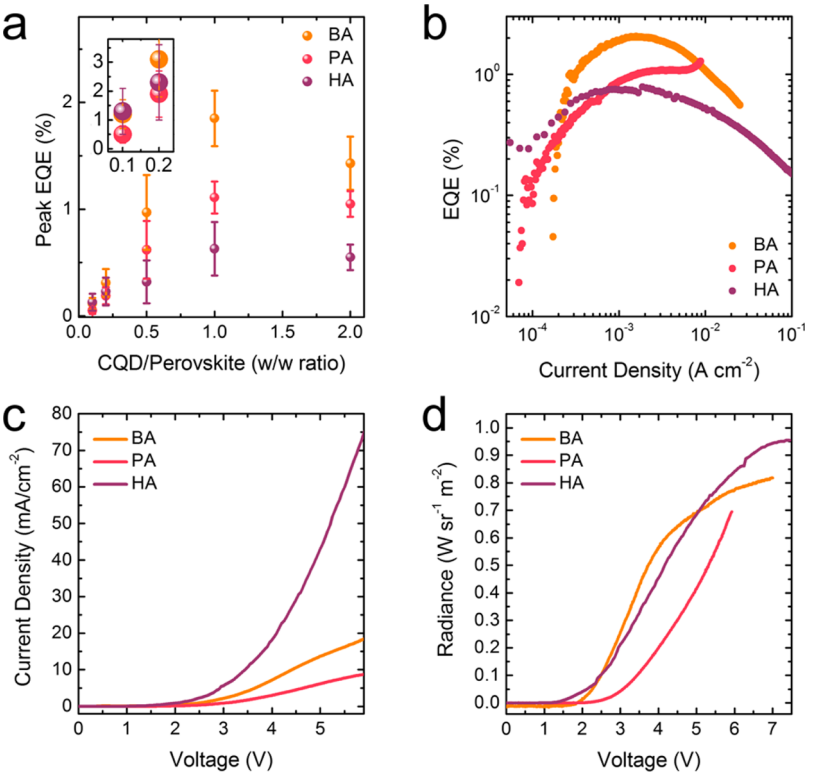


**Figure 4.** EL performance of quantum-dot-in-perovskite devices with different amine sources: (a) Average peak EQE of devices with various CQD/perovskite mass ratios (Inset: zoom-in region of EQE figure (CQD/perovskite ratio: 0.02–0.23); (b) EQE-current density performance; (c) current density–voltage curves; and (d) radiance–voltage characteristics.

the 2D perovskite type, may be better than in their 3D perovskite counterpart.

The best devices (QDs in $(BA)_2PbI_4$) had an EQE that reached 2.06% at a bias voltage of 1.35 V, and a peak radiance



DOI: 10.1021/acsphotonics.6b00865
ACS Photonics XXXX, XXX, XXX–XXX

of ∼1.5 W $sr^{-1}$ $m^{-2}$ at ∼4.1 V. Device turn-on voltages were 1.1, 1.4, and 1.3 V for the dot-in-perovskite films with BA, PA, and HA amines, respectively (Figure 4d). The high EQE value arises from the efficient charge blocking and transport provided by the F8 and $TiO_2$ charge transport layers and from the 2D perovskite passivation, which is clearly reflected in the device current density−voltage ($J$−$V$) response (Figure 4c).

It is important to note that the turn-on voltage values of these dot-in-perovskite devices were not significantly increased by the insertion of the insulating organic ligands. We propose this arise from the directional nature of charge transport from the 2D perovskite matrices to QDs. In dot-in-3D-perovskites, charge carriers are effectively captured inside individual quantum dots; the likelihood of carrier escape is low. The efficiency of the corresponding LEDs then relies on highly balanced electron−hole injection at high rates to ensure carriers will meet up before trapping/nonradiative recombination occurs. In dots-in-2D-perovskites, layered structures grow perpendicular to the substrates (Figure S8), a notion which is reflected in XRD patterns and consistent with published results of 2D perovskite thin films.[32] Charge diffusion in parallel to the octahedral $PbI_4^{2-}$ layers enhances the vertical injection of carriers from the ETL/HTL layers into the conductive $PbI_4^{2-}$ layers where carriers may then be directly transported to QDs. This significantly accelerates charge recombination in individual QDs.

## CONCLUSIONS

In this study, we fabricated QD-based NIR LEDs using a new generation of dot-in-perovskite solids as the emissive materials. The newly developed one-step surface ligand exchange effectively anchors the perovskite precursors onto the QD surfaces, where there is subsequent growth and formation of a perovskite matrix. The in situ substitution of methylammonium by other alkylammonium sources with longer carbon chains expands the perovskite lattice along the $c$-axis and therefore increases the formation energy. Both dot-in-perovskite film and device stability are substantially enhanced, allowing for devices capable of operation at higher bias. Device performance strongly depends on the length of the carbon chain in the alkylammonium building blocks, which is believed to be a key factor in adjusting the carrier mobility and maintaining the crystal stability. As a result of the optimized active layer preparation process and the insertion of the long carbon chain ammonium cations, higher QD concentrations are allowed to be embedded into the new generation of dot-in-perovskite films. Then the interface between the active layer and charge transport layers becomes much smoother, which finally yields devices with high brightness and energy conversion efficiencies.

## METHODS

**Materials.** All chemicals used are commercially available from Sigma-Aldrich (or otherwise specified) and were used without any additional purification steps: lead(II) oxide (PbO, 99.99%, from Alfa Aesar), cadmium chloride (99.99%), bis(trimethylsilyl)sulfide (synthesis grade), oleic acid (OA, tech. 90%), 1-octadecene (ODE, ≥95%), oleylamine (≥98%), dimethylformamide (DMF, 99%), octane (anhydrous, > 99%), butylamine (BA, 99.5%), pentylamine (PTA, ≥99.5%), hexylamine (HXA, ≥99%), lead(II) iodide (from Alfa Aesar, 99.999%, ultra dry), methylammonium iodide (MAI, from Dyesol Inc., 99.9%), toluene anhydrous, methanol anhydrous, acetone, distilled in glass (Caledon).

**PbS QD Synthesis and Cadmium Chloride Treatment.** The synthesis and the solution $CdCl_2$ treatment of PbS QDs followed published methods.[28,33] A total of 0.45 g PbO, 1.5 mL of OA, 18 mL of ODE, and 0.5 mL of oleylamine were loaded in a 250 mL 3-neck round-bottom flask. The mixture was then pumped at 100 °C for 60 min. After the mixed solution turned transparent, the temperature was set to 110 °C. When the solution temperature was stable at the predesigned reaction temperature, bis(trimethylsilyl)sulfide ODE solution (0.083 M) was rapidly injected into the reaction flask. The heating mantle was then turned off (but not removed) to provide slow cooling. The $CdCl_2$ treatment was carried out during the slow cooling process following a recently published method.[33] A 1 mL aliquot of $CdCl_2$ (0.06 M) oleylamine solution was injected into the QD reaction flask during the slow cooling process. At temperatures below 40 °C, QDs were precipitated by the addition of ∼50 mL of acetone and separated by ultracentrifugation. The supernatant was decanted and the nanoparticles were redispersed in 2 mL of toluene and transferred into a glovebox.

**Solution Ligand Exchange.** A 200 μL aliquot of PbS QD toluene stock solution was transferred into a clean vial and diluted to ∼5 mL with pure octane. A total of 5 mL of DMF containing equal amounts of MAI and $PbI_2$ (0.30 mol $L^{-1}$) was added into the vial and mixed vigorously at room temperature for about 2 min. After ligand exchange, CQDs were transferred from the top octane layer to the bottom DMF layer. The octane supernatant was then decanted and ∼5 mL of octane was added into the vial and mechanically mixed with the DMF solution for removing the residual long carbon chain ligands. This purification process was repeated twice and finally, the purified QD DMF solution was transferred into two test tubes (∼2.5 mL each). About 0.5 mL of toluene was added into each tube, resulting in a cloudy dark solution. The precipitate was isolated by centrifugation at 2000 rpm for 2 min and the supernatant was decanted. The precipitated QDs were dried under vacuum at room temperature for 20 min and finally redispersed into pure BA to yield a concentrated solution (∼7.5 mg/mL).

**PbS/Perovskite Precursor Mixed Solution.** A 70 μL aliquot of PbS QD BTL solution was transferred into a small centrifuge tube (1.5 mL size) and further diluted to 3.75 mg/mL by the addition of 70 μL of perovskite precursors (i.e., $PbI_2$ and $CH_3NH_3I$ with 1:1 molar ratio) in BA solution. The amount of the perovskite precursor added to the QD BTL solution was dependent on the final desired weight ratio between PbS and perovskite. For instance, for a 1:1 PbS/perovskite precursor mixed solution, 55.8 and 19.2 mg of $PbI_2$ and $CH_3NH_3I$ were dissolved in 10 mL of BA to form the perovskite precursors solution.

**Fabrication of LEDs.** Prepatterned ITO-coated glass substrates were treated using an oxygen plasma for 10 min immediately before use. The $TiO_2$ layer was fabricated by a two-step method: the initial layer was deposited at 150 °C using atomic layer deposition (ALD; Cambridge Savannah S100 ALD system) using tetrakis(dimethylamido)titanium(IV) and water as precursors, and the film was then further treated by $TiCl_4$ aqueous solutions (40 mM) at 70 °C for 30 min. This was followed by washing with deionized water, drying by $N_2$ flow, and finally, annealing at 400 °C for 1 h. Once cool, the substrates were stored in an $N_2$ glovebox for further use.


DOI: 10.1021/acsphotonics.6b00865
ACS Photonics XXXX, XXX, XXX−XXX

The PbS-perovskite precursor mixed solutions were spin-coated (6000 rpm, 30 s) onto the $TiO_2$ substrates and then annealed at 70 °C for 10 min in an $N_2$ glovebox to remove butylamine completely from the films. The F8/chlorobenzene solution (10 mg $mL^{-1}$) was annealed at 90 °C under nitrogen atmosphere and spin-cast onto the QD-in-perovskite layer at 70 °C and 3000 rpm for 60 s to form a uniform hole transport layer. The top electrode, consisting of 6 nm of $MoO_3$ and 100 nm of Ag, was deposited by thermal evaporation at a pressure $<1 \times 10^{-6}$ Torr. Each ITO substrate (2.5 cm × 2.5 cm) was patterned to yield eight devices, each with an area of 3.1 $mm^2$.

**PL and EL Measurements.** PL measurements were performed using a Horiba Fluorolog time-correlated single-photon counting system with photomultiplier tube detectors. The radiated power of EL was measured using a calibrated Ophir PD300-IR germanium photodiode (active area: 19.6 $mm^2$) and recorded in situ using a computer-controlled Keithley 2,400 source meter under a nitrogen atmosphere and in parallel with the $J-V$ measurements.

**Time-Resolved Photoluminescence Spectroscopy.** Time-resolved photoluminescence spectroscopy measurements were performed using the Horiba Fluorolog Time-Correlated Single Photon Counting (TCSPC) system equipped with UV/vis/NIR photomultiplier tube detectors, dual grating spectrometers, and a monochromatized xenon lamp excitation source. The film was placed at an incident angle of 30° away from the detector to avoid reflections of the incident beam. A 504 nm laser diode was used as a pulsed excitation source, and the time traces were acquired using the TCSPC near-infrared detector. The time window was set appropriately to ensure a complete decay of the photogenerated carriers.

**Absorption and XRD Measurements.** Optical absorption measurements were carried out in a Lambda 950500 UV−vis-IR spectrophotometer. Powder XRD patterns were collected using a Rigaku MiniFlex 600 diffractometer equipped with a NaI scintillation counter and a monochromatized Copper K$\alpha$ radiation source ($\lambda$ = 1.5406 Å).

**Device Performance Characterization.** Lambertian emission was assumed in the calculation of EQE and radiance. Peak EQE was determined as the number of forward-emitted photons to the number of injected electrons. A geometric correction factor was used according to the distance between the photodiode and device and the active area of the detector. PCE was calculated as the radiative EL power divided by the total input electrical power.

**SEM, XPS, and AFM Measurements.** SEM characterization was done on a Hitachi S-5200 scanning electron microscope. XPS analysis was carried out using Thermo Scientific K-Alpha XPS system with an Ar ion gun. AFM was done with an Asylum Research Cypher system. The AFM was operated in AC mode in air to obtain topographical and phase images. Silicon ASYELEC-01 probes with titanium−iridium coatings from Asylum Research were used for all imaging. Probes typically have a spring constant of 2 N/m.

**TEM Measurement.** High-resolution TEM and STEM-HAADF images were obtained using the Hitachi S-5200 microscope with an accelerating voltage of 300 kV. The TEM images were processed using NIH ImageJ software (version: 32-bit Java 1.6.0_24).

**TEM Sample Preparation.** The above-mentioned 1:1 PbS QD/perovskite precursor alkylamine solution was diluted five times by adding additional clean alkylamine. Inside a nitrogen-filled glovebox, ~25 $\mu$L of the precursor solution was drop-cast onto a piece of carbon coated copper TEM grid (300 mesh, Ted Pella, Inc., 01824G) and further annealed at 70 °C for 10 min under nitrogen atmosphere. When it was cooled down to room temperature, the sample grid was stored in a TEM sample holder inside the nitrogen-filled glovebox.

## ■ ASSOCIATED CONTENT

### Supporting Information

The Supporting Information is available free of charge on the ACS Publications website at DOI: 10.1021/acsphotonics.6b00865.

AFM results of the quantum-dot-in-perovskite active layer with PA and HA amines and the quantum-dot-in-perovskite film prepared following ref 16, and a table that shows XPS data regarding about elemental composition and the ratio of active materials with various amine sources (PDF).

## ■ AUTHOR INFORMATION


### Corresponding Author

*E-mail: ted.sargent@utoronto.ca.

### ORCID

Zhenyu Yang: 0000-0002-6403-8679

Oleksandr Voznyy: 0000-0002-8656-5074


### Notes

The authors declare no competing financial interest.

## ■ ACKNOWLEDGMENTS

This publication is based in part on work supported by Award KUS-11-009-21, from King Abdullah University of Science and Technology (KAUST), by the Ontario Research Fund - Research Excellence Program, and by the Natural Sciences and Engineering Research Council of Canada (NSERC). E. Yassitepe and P. Kanjanaboos are thanked for the assistance of HRTEM, STEM, and AFM measurements. The authors thank L. Gao, R. Wolowiec, D. Kopilovic, and E. Palmiano for their help and useful discussions.

## ■ REFERENCES


(1) Efros, A. L. Interband absorption of light in a semiconductor sphere. *Soviet Physics Semiconductors-Ussr* **1982**, *16*, 772−775.

(2) Rossetti, R.; Nakahara, S.; Brus, L. E. Quantum size effects in the redox potentials, resonance Raman spectra, and electronic spectra of CdS crystallites in aqueous solution. *J. Chem. Phys.* **1983**, *79*, 1086−1088.

(3) Colvin, V. L.; Schlamp, M. C.; Alivisatos, A. P. Light-emitting diodes made from cadmium selenide nanocrystals and a semiconducting polymer. *Nature* **1994**, *370*, 354−357.

(4) Dabbousi, B. O.; Bawendi, M. G.; Onitsuka, O.; Rubner, M. F. Electroluminescence from CdSe quantum-dot/polymer composites. *Appl. Phys. Lett.* **1995**, *66*, 1316−1318.

(5) Coe, S.; Woo, W.-K.; Bawendi, M.; Bulovic, V. Electroluminescence from single monolayers of nanocrystals in molecular organic devices. *Nature* **2002**, *420*, 800−803.

(6) Tessler, N.; Medvedev, V.; Kazes, M.; Kan, S.; Banin, U. Efficient Near-Infrared Polymer Nanocrystal Light-Emitting Diodes. *Science* **2002**, *295*, 1506−1508.

(7) Sargent, E. H. Infrared Quantum Dots. *Adv. Mater.* **2005**, *17*, 515−522.

(8) Anikeeva, P. O.; Halpert, J. E.; Bawendi, M. G.; Bulović, V. Quantum Dot Light-Emitting Devices with Electroluminescence Tunable over the Entire Visible Spectrum. *Nano Lett.* **2009**, *9*, 2532−2536.




DOI: 10.1021/acsphotonics.6b00865
*ACS Photonics* XXXX, XXX, XXX−XXX

(9) Shirasaki, Y.; Supran, G. J.; Bawendi, M. G.; Bulovic, V. Emergence of colloidal quantum-dot light-emitting technologies. *Nat. Photonics* **2012**, *7*, 13−23.
(10) Bourdakos, K. N.; Dissanayake, D. M. N. M.; Lutz, T.; Silva, S. R. P.; Curry, R. J. Highly efficient near-infrared hybrid organic-inorganic nanocrystal electroluminescence device. *Appl. Phys. Lett.* **2008**, *92*, 153311.
(11) Choudhury, K. R.; Song, D. W.; So, F. Efficient solution-processed hybrid polymer−nanocrystal near infrared light-emitting devices. *Org. Electron.* **2010**, *11*, 23−28.
(12) Ma, X.; Xu, F.; Benavides, J.; Cloutier, S. G. High performance hybrid near-infrared LEDs using benzenedithiol cross-linked PbS colloidal nanocrystals. *Org. Electron.* **2012**, *13*, 525−531.
(13) Sun, L.; Choi, J. J.; Stachnik, D.; Bartnik, A. C.; Hyun, B.-R.; Malliaras, G. G.; Hanrath, T.; Wise, F. W. Bright infrared quantum-dot light-emitting diodes through inter-dot spacing control. *Nat. Nanotechnol.* **2012**, *7*, 369−373.
(14) Supran, G. J.; Song, K. W.; Hwang, G. W.; Correa, R. E.; Scherer, J.; Dauler, E. A.; Shirasaki, Y.; Bawendi, M. G.; Bulović, V. High-Performance Shortwave-Infrared Light-Emitting Devices Using Core−Shell (PbS−CdS) Colloidal Quantum Dots. *Adv. Mater.* **2015**, *27*, 1437−1442.
(15) Krames, M. R.; Shchekin, O. B.; Mueller-Mach, R.; Mueller, G. O.; Zhou, L.; Harbers, G.; Craford, M. G. Status and Future of High-Power Light-Emitting Diodes for Solid-State Lighting. *J. Disp. Technol.* **2007**, *3*, 160−175.
(16) Gong, X.; Yang, Z.; Walters, G.; Comin, R.; Ning, Z.; Beauregard, E.; Adinolfi, V.; Voznyy, O.; Sargent, E. H. Highly efficient quantum dot near-infrared light-emitting diodes. *Nat. Photonics* **2016**, *10*, 253−257.
(17) Semonin, O. E.; Johnson, J. C.; Luther, J. M.; Midgett, A. G.; Nozik, A. J.; Beard, M. C. Absolute Photoluminescence Quantum Yields of IR-26 Dye, PbS, and PbSe Quantum Dots. *J. Phys. Chem. Lett.* **2010**, *1*, 2445−2450.
(18) Zhitomirsky, D.; Voznyy, O.; Hoogland, S.; Sargent, E. H. Measuring charge carrier diffusion in coupled colloidal quantum dot solids. *ACS Nano* **2013**, *7*, 5282−5290.
(19) Choi, J. J.; Luria, J.; Hyun, B.-R.; Bartnik, A. C.; Sun, L.; Lim, Y.-F.; Marohn, J. A.; Wise, F. W.; Hanrath, T. Photogenerated Exciton Dissociation in Highly Coupled Lead Salt Nanocrystal Assemblies. *Nano Lett.* **2010**, *10*, 1805−1811.
(20) Greenham, N. C.; Peng, X.; Alivisatos, A. P. Charge separation and transport in conjugated-polymer/semiconductor-nanocrystal composites studied by photoluminescence quenching and photoconductivity. *Phys. Rev. B: Condens. Matter Mater. Phys.* **1996**, *54*, 17628−17637.
(21) Steckel, J. S.; Coe-Sullivan, S.; Bulović, V.; Bawendi, M. G. 1.3 to 1.55 $\mu$m Tunable Electroluminescence from PbSe Quantum Dots Embedded within an Organic Device. *Adv. Mater.* **2003**, *15*, 1862−1866.
(22) Moroz, P.; Liyanage, G.; Kholmicheva, N. N.; Yakunin, S.; Rijal, U.; Uprety, P.; Bastola, E.; Mellott, B.; Subedi, K.; Sun, L.; Kovalenko, M. V.; Zamkov, M. Infrared Emitting PbS Nanocrystal Solids through Matrix Encapsulation. *Chem. Mater.* **2014**, *26*, 4256−4264.
(23) Ning, Z.; Gong, X.; Comin, R.; Walters, G.; Fan, F.; Voznyy, O.; Yassitepe, E.; Buin, A.; Hoogland, S.; Sargent, E. H. Quantum-dot-in-perovskite solids. *Nature* **2015**, *523*, 324−328.
(24) Buin, A.; Pietsch, P.; Xu, J.; Voznyy, O.; Ip, A. H.; Comin, R.; Sargent, E. H. Materials Processing Routes to Trap-Free Halide Perovskites. *Nano Lett.* **2014**, *14*, 6281−6286.
(25) Saparov, B.; Mitzi, D. B. Organic−Inorganic Perovskites: Structural Versatility for Functional Materials Design. *Chem. Rev.* **2016**, *116*, 4558−4596.
(26) Quan, L. N.; Yuan, M.; Comin, R.; Voznyy, O.; Beauregard, E. M.; Hoogland, S.; Buin, A.; Kirmani, A. R.; Zhao, K.; Amassian, A.; Kim, D. H.; Sargent, E. H. Ligand-Stabilized Reduced-Dimensionality Perovskites. *J. Am. Chem. Soc.* **2016**, *138*, 2649−2655.
(27) Yang, Z.; Yassitepe, E.; Voznyy, O.; Janmohamed, A.; Lan, X.; Levina, L.; Comin, R.; Sargent, E. H. Self-Assembled PbSe Nanowire: Perovskite Hybrids. *J. Am. Chem. Soc.* **2015**, *137*, 14869−14872.
(28) Hines, M. A.; Scholes, G. D. Colloidal PbS Nanocrystals with Size-Tunable Near-Infrared Emission: Observation of Post-Synthesis Self-Narrowing of the Particle Size Distribution. *Adv. Mater.* **2003**, *15*, 1844−1849.
(29) Billing, D. G.; Lemmerer, A. Synthesis, characterization and phase transitions in the inorganic-organic layered perovskite-type hybrids [(CnH2n + 1NH3)2PbI4], n = 4, 5 and 6. *Acta Crystallogr., Sect. B: Struct. Sci.* **2007**, *63*, 735−747.
(30) Calloni, A.; Abate, A.; Bussetti, G.; Berti, G.; Yivlialin, R.; Ciccacci, F.; Duò, L. Stability of Organic Cations in Solution-Processed CH3NH3PbI3 Perovskites: Formation of Modified Surface Layers. *J. Phys. Chem. C* **2015**, *119*, 21329−21335.
(31) Liu, L.; McLeod, J. A.; Wang, R.; Shen, P.; Duhm, S. Tracking the formation of methylammonium lead triiodide perovskite. *Appl. Phys. Lett.* **2015**, *107*, 061904.
(32) Cao, D. H.; Stoumpos, C. C.; Farha, O. K.; Hupp, J. T.; Kanatzidis, M. G. 2D Homologous Perovskites as Light-Absorbing Materials for Solar Cell Applications. *J. Am. Chem. Soc.* **2015**, *137*, 7843−7850.
(33) Yang, Z.; Voznyy, O.; Liu, M.; Yuan, M.; Ip, A. H.; Ahmed, O. S.; Levina, L.; Kinge, S.; Hoogland, S.; Sargent, E. H. All-Quantum-Dot Infrared Light-Emitting Diodes. *ACS Nano* **2015**, *9*, 12327−12333.
(34) Comin, R.; Walters, G.; Thibau, E. S.; Voznyy, O.; Lu, Z.-H.; Sargent, E. H. Structural, optical, and electronic studies of wide-bandgap lead halide perovskites. *J. Mater. Chem. C* **2015**, *3*, 8839−8843.
(35) Safdari, M.; Svensson, P. H.; Hoang, M. T.; Oh, I.; Kloo, L.; Gardner, J. M. Layered 2D alkyldiammonium lead iodide perovskites: synthesis, characterization, and use in solar cells. *J. Mater. Chem. A* **2016**, *4*, 15638−15646.


DOI: 10.1021/acsphotonics.6b00865
*ACS Photonics* XXXX, XXX, XXX−XXX